

# Degradation of Lignosulfonate to Vanillic Acid Using Ferrate

Jana Klein, Robin Kupec, Markus Stöckl,\* and Siegfried R. Waldvogel\*

A new method is presented using electrochemically generated ferrate to degrade the technically relevant bio-based side-stream products, lignin and lignosulfonate. An exclusive degradation to vanillic acid is found, which was previously a reported by-product. As a natural resource, lignin can be utilized to substitute fossil-based chemicals in the industry to reduce greenhouse gas emissions and positively impact climate change. Ferrate is generated from grey cast iron sacrificial anodes in 40 wt% NaOH with a current efficiency of over 22% at a current density of up to 100 mA cm<sup>-2</sup>. Vanillic acid is obtained as the sole product after optimizing the reaction parameters, temperature, time, and ferrate concentration for the lignosulfonate degradation via the design of experiments. As a result, yields of 7.2 wt% of the flavoring agent and antioxidant vanillic acid are achieved. The presented two-step degradation provides an inexpensive path for the production of vanillic acid on a laboratory scale from a highly abundant bio-based side-stream.

high technical interest as renewable and bio-based feedstock<sup>[7]</sup> due to their aromatic backbone and high availability.<sup>[8–11]</sup> Consequently, the targeted degradation of the respective lignin fractions to value-added products is highly desired.<sup>[12,13]</sup> The difficulty of this process lies in the different functionalization and the structure of the polyphenolic backbone, which depends on many factors such as pulping process, harvesting time, and type of tree.<sup>[10,14]</sup> Therefore, the industry uses only small fractions for further production, while the majority is incinerated to recover energy costs.<sup>[4,9]</sup> Lignin, as a renewable feedstock, offers a promising alternative to petroleum refining and shows tremendous potential for bio-based products such as surfactants and fine chemicals.<sup>[5,13,15]</sup>

Nevertheless, selective degradation is challenging, and several studies focused

on this complex topic to degrade lignin into value-added products such as aromatic intermediates.<sup>[8,16–18]</sup> Lignin degradation shows a broad and diverse spectrum of products, such as aldehydes,<sup>[19–21,22]</sup> alcohols,<sup>[21]</sup> arenes,<sup>[18,23,24]</sup> quinones,<sup>[25]</sup> and carboxylic acids,<sup>[16,26,27]</sup> obtained in previous research. Different metal-based catalysts were studied to improve degradation and increase selectivity including noble metals like ruthenium, palladium, and platinum.<sup>[28]</sup> The disadvantages of these processes are the very high costs and limited availability of the metals, which might also cause uncontrolled over-hydrogenation, decreasing the yield of the phenolic products. Another approach is using ionic liquids as solvents in combination with catalysts or oxidizers.<sup>[29]</sup> However, the high costs for ionic liquids restrict their application for industrial operations. Additionally, the separation process is complex due to interactions with aromatic moieties of residual lignin.

Promising electrochemical pathways are reported to yield aldehydes,<sup>[3,21,30]</sup> carboxylic acids,<sup>[27,31]</sup> and other phenolic products in good yields.<sup>[19,21,27,30]</sup> These methods are cost-effective and environmentally friendly.<sup>[32]</sup> Also, a well-known alternative is the use of oxidizers for lignin degradation.<sup>[3,20,23]</sup> However, only a few oxidizers, such as periodate,<sup>[3]</sup> nitrobenzene,<sup>[33,34]</sup> or hydrogen peroxide,<sup>[35]</sup> have high availability, and are safe in handling. Moreover, lignin conversion is not limited to the electrode surface since the respective oxidizers are dissolved. The monomer yields out of lignin using oxidizers vary significantly due to different wood types and experimental conditions. In a previous report, we showed that platform oxidizers, such as periodate, are highly beneficial for lignin degradation. This method significantly improves the vanillin yield (8.9 wt%) or selectively produces 5-iodovanillin using different workup conditions.<sup>[3]</sup>

## 1. Introduction


In nature, lignin is the most abundant aromatic polymer and can be exploited as a renewable feedstock.<sup>[1]</sup> Worldwide technical lignins are produced annually in large quantities (100 million tons)<sup>[2]</sup> as a side-stream product of the pulp and paper industry.<sup>[3–5]</sup>

Approximately 10% of the total lignin output are lignosulfonates,<sup>[6]</sup> whereas the rest consists of Kraft lignin. Both are of

J. Klein, S. R. Waldvogel  
 Department of Chemistry  
 Johannes Gutenberg University  
 Duesbergweg 10–14, 55128 Mainz, Germany  
 E-mail: waldvogel@uni-mainz.de

R. Kupec, M. Stöckl  
 Department of Chemical Technology  
 DECHEMA-Forschungsinstitut  
 Theodor-Heuss-Allee 25, 60486 Frankfurt am Main, Germany  
 E-mail: markus.stoeckl@dechema.de

S. R. Waldvogel  
 Institute of Biological and Chemical Systems – Functional Molecular Systems (IBCS-FMS)  
 Hermann-von-Helmholtz-Platz 1  
 76344 Eggenstein-Leopoldshafen, Germany

 The ORCID identification number(s) for the author(s) of this article can be found under <https://doi.org/10.1002/adsu.202200431>.

© 2022 The Authors. Advanced Sustainable Systems published by Wiley-VCH GmbH. This is an open access article under the terms of the Creative Commons Attribution-NonCommercial-NoDerivs License, which permits use and distribution in any medium, provided the original work is properly cited, the use is non-commercial and no modifications or adaptations are made.

DOI: 10.1002/adsu.202200431

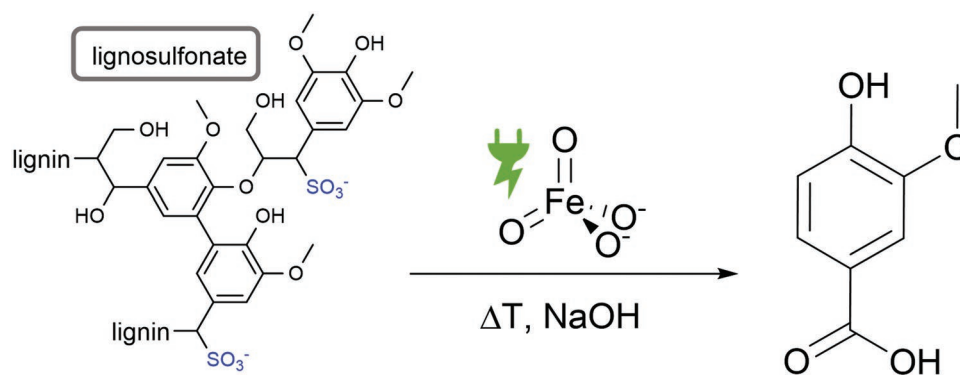


**Figure 1.** Lignin degradation with electrochemically generated ferrate to vanillic acid.

This study presents the degradation of lignin and lignosulfonate with electrochemically generated ferrate (**Figure 1**). Ferrate refers to iron in its highest oxidation state Fe(VI), which can be obtained via wet chemical, thermal, or electrochemical oxidation of Fe(III) species.<sup>[36–39]</sup> Due to its decent oxidation potential and low toxicity, ferrate has gained increasing interest in wastewater treatment,<sup>[40–43]</sup> where it can function as a green oxidizer, disinfectant, and coagulant in the same process.<sup>[38,44]</sup> However, the practical application remains challenging, mainly since ferrate is only metastable in highly alkaline conditions limiting its use in wastewater treatment.<sup>[36,45,46]</sup> Moreover, conventional chemical synthesis of ferrate requires hypochlorite, which diminishes the advantage of using a green oxidizer.<sup>[36–40]</sup>

If prepared via an electrochemical route, ferrate can be obtained by anodic oxidation of iron in alkaline media without needing additional reagents.<sup>[42,47–53]</sup> Numerous studies have shown that iron electrodes with high carbon content, such as grey cast iron (GCI), are ideally suited as sacrificial anodes.<sup>[40,47,48]</sup> It was postulated that carbon in the form of carbide in iron anodes reduces the stability of the passivation layer and thus improves ferrate electro-generation.<sup>[54]</sup> Earlier research varies regarding the electrolytes where base concentrations of 10 to 16 M NaOH and KOH can be found. Multiple reports suggest that 14 M NaOH is optimal to maximize ferrate generation.<sup>[50,53,54]</sup>

While such high base concentrations are detrimental to the application of ferrate in wastewater treatment, they are ideal conditions for the thermal degradation of lignin. As such, we combined electrochemical ferrate generation with thermal lignin degradation to improve the latter by using the green oxidant ferrate. Using ferrate as enhancing oxidizer, we generate vanillic acid as a new and underestimated degradation product. It is also used, as vanillin, as a food additive.<sup>[55,56]</sup> Many studies emphasize its antioxidant and antimicrobial properties.<sup>[56,57]</sup>

## 2. Results and Discussion

A new, cost-efficient, sustainable method has been developed for preparing vanillic acid (**1**) out of the source lignin. The price of vanillic acid is more than ten times higher than that of vanillin.<sup>[58,59]</sup> Compared to existing publications, our starting material is not vanillin but inexpensive lignin and lignosulfonate

with high accessibility on a multi-million-ton scale.<sup>[60]</sup> For vanillin's well-known oxidation, expensive or toxic oxidizing agents, such as silver oxide<sup>[61,62]</sup> or nitrobenzene,<sup>[61]</sup> are needed. Also, caustic fusion needs high alkaline solutions and even higher temperatures.<sup>[63]</sup> Therefore, inexpensive ferrate as a green oxidizer supports the oxidation of waste-stream lignins and can skip the step from vanillin to vanillic acid. Compared to the literature, no lignin oxidation is known just for selective vanillic acid production. Either vanillic acid appears as a by-product in low yields or traces of model compounds are used.<sup>[64]</sup> Further, the use of microbial cells to convert vanillin or ferulic acid to vanillic acids is known.<sup>[59,65]</sup>

For this reaction, a two-step process is designed. Initially, ferrate is electrochemically generated in alkaline aqueous media at room temperature in a membrane-separated cell (**Figure 5**). The ferrate oxidation occurs at a GCI electrode, and the reduction is performed at a stainless steel electrode for a smooth counter-reaction (hydrogen evolution reaction, HER).<sup>[66]</sup> Ferrate is subsequently transferred in an autoclave containing lignin (**Figure 6**). Vanillic acid (**1**) is formed selectively out of lignin in high yields by using ferrate as the oxidizing agent.

### 2.1. Influence of NaOH Concentration on Electro-Generation of Ferrate

This work aimed to produce dissolved ferrate in high concentrations and with good current efficiencies (CE) while maintaining industrial-relevant current densities. GCI was chosen as the sacrificial anode material because it is already well-studied and proven to be suited for ferrate generation due to its high carbon content.<sup>[40,47,48]</sup>

To optimize ferrate electro-generation, the influence of NaOH concentration, ranging from 10 wt% (2.8 M) up to 50 wt% (19 M), was investigated in 2 h screening experiments (**Figure 2a**). In our previous work, we reported that 3 M NaOH is sufficient for the thermal degradation of lignin assisted by periodate to obtain vanillin or iodovanillin in high yields.<sup>[3]</sup> Therefore, NaOH concentrations as low as 10 wt% (2.8 M) were tested for the electro-generation of ferrate to reduce corrosiveness and cost.

**Figure 2a** depicts the production of ferrate during the anodic oxidation of GCI in different NaOH concentrations at

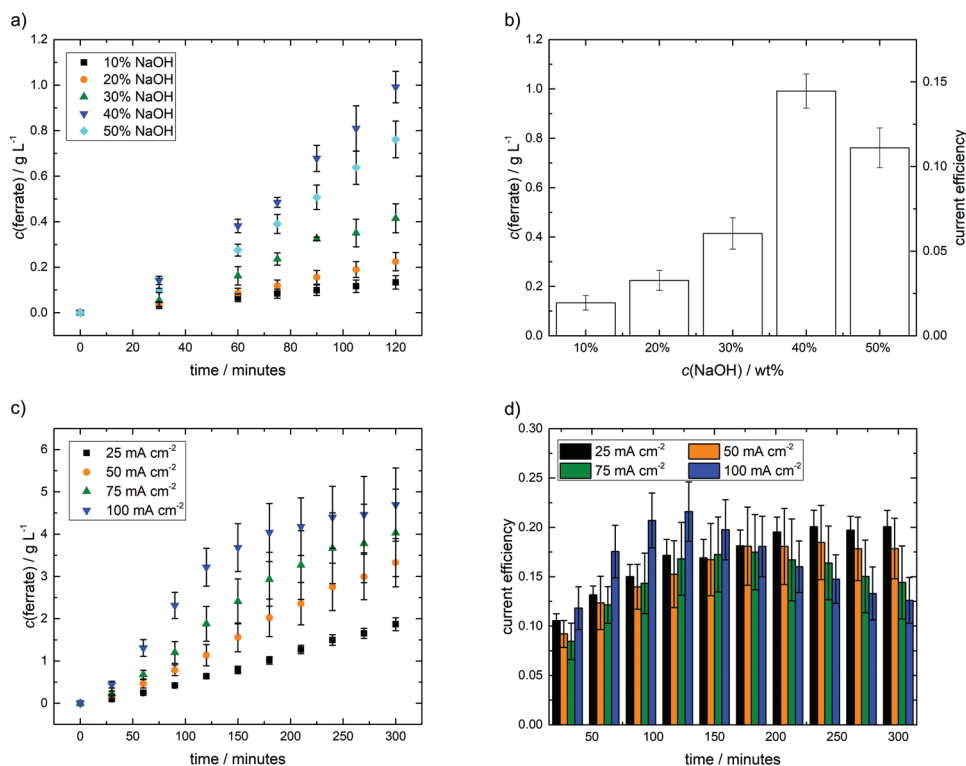


**Figure 2.** Ferrate electro-generation at GCI in NaOH: a) Ferrate concentration over 120 min for 10, 20, 30, 40, and 50 wt% NaOH at  $j = 50 \text{ mA cm}^{-2}$ , b) peak concentration and current efficiency after 120 min of (a), c) ferrate concentration over 300 min in 40 wt% NaOH at  $j = 25, 50, 75,$  and  $100 \text{ mA cm}^{-2}$ , and d) current efficiency over time in 40 wt% NaOH at  $j = 25, 50, 75,$  and  $100 \text{ mA cm}^{-2}$ .

a constant current density ( $j = 50 \text{ mA cm}^{-2}$ ) over 2 h. Despite possible advantages, 10 (2.8 M) to 30 wt% NaOH (10 M) proved to be insufficient for ferrate generation at acceptable current efficiencies with  $1.8 \pm 0.4\%$ ,  $3.0 \pm 0.5\%$ , and  $5.6 \pm 0.7\%$ , respectively (Figure 2b). The maximum ferrate concentration after 2 h of  $0.99 \pm 0.07 \text{ g L}^{-1}$  was achieved in 40 wt% (14 M) NaOH, followed by  $0.76 \pm 0.08 \text{ g L}^{-1}$  in 50 wt% NaOH (19 M) with current efficiencies of  $13.3 \pm 0.1\%$  and  $10.8 \pm 0.1\%$ , respectively (Figure 2b). Considering that the electrochemical formation of ferrate in alkaline media from sacrificial anodes consumes vast amounts of  $\text{OH}^-$ ,<sup>[67]</sup> one would expect the highest ferrate concentration in 50 wt% NaOH with decreasing performance in lower base concentrations. However, this is not the case with 50 wt% NaOH being almost twice as efficient as 30 wt% but about 20% less efficient than 40 wt% NaOH (Figure 2b). This trend is likely explained by the varying electrical conductivities and the resulting terminal voltages in different concentrations of NaOH (Figure S3, Supporting Information). 10, 20, and 30 wt% NaOH have very high electrical conductivity ( $358, 414,$  and  $292 \text{ mS cm}^{-1}$ , respectively)<sup>[68]</sup> and, as such, relatively low terminal voltage during electrolysis experiments (Figure S3, Supporting Information) but likely insufficient  $\text{OH}^-$  concentration for efficient ferrate generation. While 40 and 50 wt% NaOH provide more  $\text{OH}^-$  for the reaction, their electrical conductivities are lower. The performance difference between 50 wt% NaOH ( $150 \text{ mS cm}^{-1}$ )<sup>[68]</sup> and 40 wt% NaOH ( $191 \text{ mS cm}^{-1}$ )<sup>[68]</sup> is possibly explained by the resulting terminal voltages being  $\approx 30\%$  higher for 50 wt% NaOH (Figure S3,

Supporting Information), increasing thermal losses and favoring side reactions such as oxygen evolution reaction (OER). The higher viscosity of 50 wt% NaOH probably hinders diffusion to the electrode surface, further decreasing performance. 40 wt% NaOH appears to be the ideal compromise between  $\text{OH}^-$  concentration, conductivity, and viscosity. These findings are in agreement with the literature where suitable NaOH concentrations ranging from 30 (10 M) to 44 wt% (16 M) can be found depending on exact experimental setups, with multiple reports suggesting 40 wt% (14 M) NaOH being the ideal concentration.<sup>[42,43,47,51,53]</sup>

## 2.2. Impact of Current Density Variation of Ferrate Production

40 wt% NaOH was shown to be the best electrolyte tested in this study and was further investigated by testing different current densities to optimize ferrate generation. Electrolysis at current densities of  $j = 25, 50, 75,$  and  $100 \text{ mA cm}^{-2}$  ( $A_{\text{anode}} = 10 \text{ cm}^2$ ) have been carried out for 5 h (Figure 2c).

Looking at the error bars, it is immediately apparent that reproducibility in these experiments was challenging. Standard deviation seems to increase with current density and electrolysis time, leading to overlapping error bars after 2 h.

Nevertheless, the data presented in Figure 2c,d still show significant trends in the electrolysis performance despite the standard deviations. For  $j = 25$  and  $50 \text{ mA cm}^{-2}$ , ferrate concentration increases almost exponentially until 210 and 180 min,

respectively, corresponding to an initial increase in current efficiency followed by a constant value (around 20% and 18%). This behavior might be rationalized by the dissolving of the initially smooth electrode leading to a coarse surface with a larger area more suited for efficient diffusion. Experiments with  $j = 25 \text{ mA cm}^{-2}$  revealed high reproducibility, low standard deviation, and decent current efficiency of around 20%. However, the production rate of ferrate was found to be insufficient for this work.

For  $j = 75$  and  $100 \text{ mA cm}^{-2}$ , the same initial increase in current efficiency was observed. However, this did not lead to a constant value but a substantial drop resulting in increasingly stagnating ferrate production. In the case of  $j = 100 \text{ mA cm}^{-2}$ , the experiments exhibited promising results with the highest current efficiency for the first 120 min and a peak efficiency of  $22 \pm 3\%$  resulting in a ferrate concentration of  $3.2 \pm 0.5 \text{ g L}^{-1}$ . After that, the CE decreased approximately linearly to  $13 \pm 2\%$  at 300 min, thus inferior to the other tested current densities. Nevertheless, the significantly higher initial CE compared to the three lower current densities still resulted in the highest ferrate concentration after 5 h with  $4.7 \pm 0.9 \text{ g L}^{-1}$  despite the steep decline of CE in the latter half of the electrolysis at  $100 \text{ mA cm}^{-2}$ .

For short-term ferrate electro-generation, it was shown that increasing current densities led to higher current efficiencies and satisfactory total ferrate amounts usable for further applications like lignin degradation. For prolonged electrolysis, however, electrodes seem to undergo passivation, which is accelerated with increasing current densities and severely hinders the application of the process regarding continuous and possibly scaled-up electrochemical ferrate production.

### 2.3. Electrode Passivation

The passivation of sacrificial iron anodes during ferrate electro-generation is widely discussed in the literature. It is identified as one of the most challenging problems for the long-term generation of ferrate. The discussions mainly focus on the formation of ferric oxide layers during electrolysis, which is said to persist on the electrode surface, hindering the diffusion of electrolytes to active iron sites.<sup>[40,43,47–49,53,67,69]</sup>

Passivation was also observed during electrolysis at  $75 \text{ mA cm}^{-2}$  and more pronounced at  $100 \text{ mA cm}^{-2}$ . Figure 2d displays a rapid decline of current efficiency, and consequently, stagnation of ferrate generation after 150 min (Figure 2c). To investigate this phenomenon, three GCI electrodes used for the experiments at  $100 \text{ mA cm}^{-2}$  for 5 h in 40 wt% NaOH were analyzed by scanning electron microscopy (SEM) before and after electrolysis (Figures S7–S23, Supporting Information). Multiple images of secondary electrons (SE) and backscattered electrons (BSE) were taken and further analyzed by energy-dispersive X-ray spectroscopy (EDX, Tables S9–S14, Supporting Information). The analysis of the electrode surface suggested a form of passivation, that is, as far as we know, only discussed by Bouzek et al. and is specific to iron electrodes with high graphitic carbon contents such as GCI.<sup>[40,49]</sup> SEM images at 150× magnification (Figure 3a and 3c and Figures S10, S12, S20, and S22, Supporting Information) show a highly coarse surface, as would be expected after electrolysis of a sacrificial anode in comparison to the initially smooth surfaces (Figures S9 and S19, Supporting Information). Figure 3b represents the

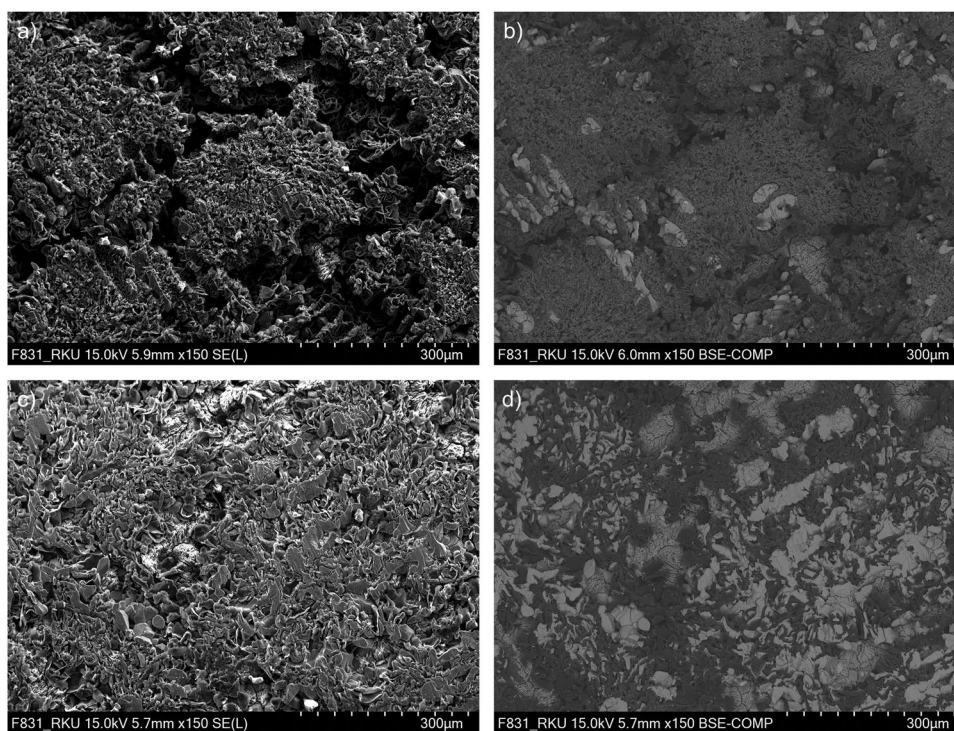


**Figure 3.** SEM images of GCI electrodes after electrolysis in 40 wt% NaOH for 300 min: a) SE image of electrode GCI2.12 at 150× magnification, b) BSE image of electrode GCI2.12 at 150× magnification, c) SE image of electrode GCI2.19 at 150× magnification, and d) BSE image of electrode GCI2.19 at 150× magnification.

BSE image of Figure 3a, clearly showing that almost all iron (light grey; confirmed by EDX, Figure S11 and Table S9, Supporting Information) from the electrode surface is gone. It presumably was transformed into ferrate or other ferric oxides no longer present on the electrode surface. The remaining is primarily pure carbon (dark grey; confirmed by EDX, Figure S11 and Table S9, Supporting Information), which is neither dissolved nor mineralized under the applied electrolysis conditions in the given time. It is most likely performing OER, thus leading to rapidly declining electrode performance concerning ferrate generation, as suspected by Bouzek et al.<sup>[40,49]</sup> This hypothesis is further supported by the decrease in terminal voltage and constant anodic half-cell potential (HCP) over the electrolysis time as opposed to an increase, which would be expected during conventional passivation with ferric oxides (Figures S4 and S5, Supporting Information). To investigate this mechanism further, we conducted linear sweep voltammetry (LSV) on novel GCI, and pure graphite and used GCI electrodes in 40 wt% NaOH (Figure S6, Supporting Information). Anodic HCP measurements during the electrolysis of GCI in 40 wt% NaOH over 5 h showed a stable potential of around  $1000 \pm 100$  mV versus SHE after an initial exponential decrease (Figure S5, Supporting Information). Considering the Pourbaix diagram of iron based on  $1 \text{ mol L}^{-1}$  ferrate in an aqueous solution at  $25^\circ\text{C}$  published by Wulfsberg, our value is within the range of possible ferrate generation.<sup>[70]</sup> It is postulated that ferrate can be generated at  $\text{pH} = 14$  between the Fe(VI)/Fe(III) standard reduction potential of  $0.71 \text{ V}$  versus SHE and the necessarily applied potential to oxidize  $\text{H}_2\text{O}$  at  $1.21 \text{ V}$  versus SHE, assuming  $+0.5 \text{ V}$  of over-potential.<sup>[46,70]</sup> However, in our practical application, a novel GCI electrode showed an exponential increase in current, reminiscent of OER, starting at  $750 \text{ mV}$  versus SHE without a distinguishable ferrate peak during LSV (Figure S6, Supporting Information). These findings explain the generally low current efficiencies because ferrate generation competes with OER under the applied conditions. However, avoiding OER altogether seems impractical because an applied potential of  $710 \text{ mV}$  versus SHE would only result in a current density of  $1 \text{ mA cm}^{-2}$  (Figure S6, Supporting Information). We suspect the discrepancy compared to the theoretical values is caused by the many impurities in GCI, especially the high graphitic carbon content. Pure graphite shows OER onset during LSV in 40 wt% NaOH as low as  $200 \text{ mV}$  versus SHE and very clearly at  $500 \text{ mV}$  versus SHE (Figure S6, Supporting Information). We established with SEM that our electrode surfaces become more graphitic during ferrate electro-generation expecting a shift toward OER while maintaining terminal voltage and HCP. This hypothesis can be confirmed with LSV showing that used GCI electrodes (after electrolysis in 40 wt% NaOH for 5 h) exhibit an earlier OER onset potential of around  $700 \text{ mV}$  versus SHE, a decrease of  $50 \text{ mV}$  compared to a novel GCI rod (Figure S6, Supporting Information).

At the same time, these findings explain the relatively poor reproducibility and high standard deviations during repeated experiments. Comparing the SEM/BSE images of the worst (Figure 3a,b:  $c_{t=5\text{h}}(\text{ferrate}) = 4.1 \text{ g L}^{-1}$ ) and best (Figure 3c,d:  $c_{t=5\text{h}}(\text{ferrate}) = 5.7 \text{ g L}^{-1}$ ) performing electrode, it is apparent that the orientation of carbon and the amount of remaining iron (and iron oxides) on the surfaces is different.

The worst-performing electrode shows a layer of carbon parallel to the original surface (see also Figures S10 and S12, Supporting Information), which leads to a steep decline in ferrate generation and presumably a shift toward parasitic OER. The best-performing electrode shows fewer carbon deposits, which also appear in a different orientation, perpendicular to the original surface (see also Figures S20 and S22, Supporting Information). This formation still allows electrolyzation of the iron surface, further dissolving the electrode and ongoing ferrate synthesis. The average performing electrode exhibits properties of both with islands of smooth, low surface area iron scattered among large carbon deposits parallel to the surface (Figures S15–S18 and Tables S11 and S12, Supporting Information). These findings suggest that inhomogeneous materials containing flake graphite, such as 0.6025 GCI, behave unpredictably in repeated experiments and might not be optimal for long-term ferrate generation. On the other hand, Diaz et al. successfully implemented GCI in short-term ferrate generation, vastly outperforming white cast iron (WCI) even though Bouzek et al. suggested WCI to be superior due to its high carbide content.<sup>[40,49,51,67]</sup> However, comparing different studies is challenging if exact material numbers, therefore composition appearing iron and graphite phases, and resulting material properties are unknown. Together with our findings, we conclude that cast iron with flake graphite should be avoided for long-term electrolysis, and alternatives with carbon contents in between mild steel ( $\text{C} = 0.05\text{--}0.25\%$ ) and cast iron ( $\text{C} > 2\%$ ) should be further investigated. Such research might lead to the discovery of an ideal compromise in carbon content that allows for sufficient catalytical activity while minimizing passivation.

#### 2.4. Lignin Oxidation with Electrochemically Generated Ferrate as the Oxidizer

The reaction of pure vanillin to vanillic acid in highly alkaline media is already known.<sup>[71]</sup> The reaction occurs within 45 min at  $150^\circ\text{C}$  in potassium hydroxide solution ( $8.25 \text{ g L}^{-1}$ ). Since 40 wt% NaOH has shown to be ideally suited for efficient ferrate electro-generation, the same concentration was used for lignin degradation under the assumption that formed vanillin is directly overoxidized to the corresponding acid in a single step. We hypothesized that ferrate as a potent oxidizing agent would aid the reaction by reacting with the lignin polymer, increasing product yields analog to our previous work in which periodate could improve vanillin yields. Therefore, lignosulfonate was chosen as the test substrate due to its potential vanillin units, confirmed by the nitrobenzene oxidation performed as a reference reaction (further information provided in Supporting Information, GP3).<sup>[34,72]</sup> After the positive effect of ferrate on lignosulfonate degradation, optimization was carried out using a design of experiments (DoE) approach.<sup>[73]</sup> An investigation of three different parameters was conducted: degradation time, reaction temperature, and concentration of ferrate. For the optimization, 34 experiments with lignosulfonate were performed (Table S4, Supporting Information). The investigated time range for the reaction was between 2 and 16 h. Due to the experience that lignin degradations performed at  $120^\circ\text{C}$  showed low yields, a temperature range between  $140$  and

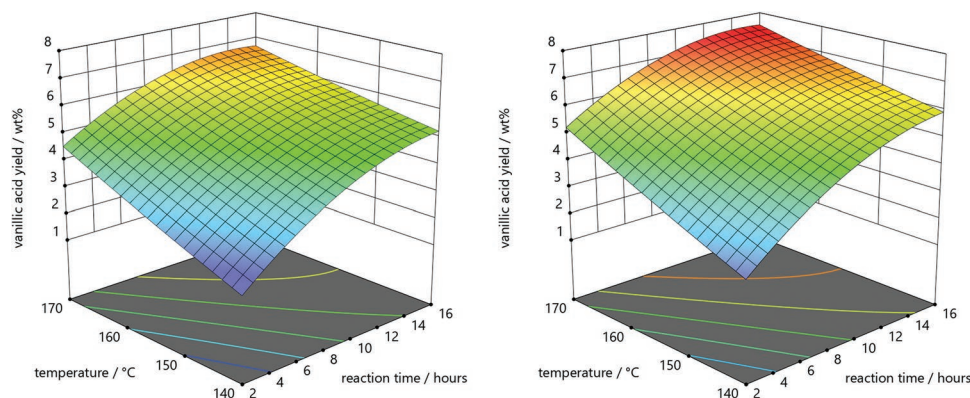


**Figure 4.** 3D-Plots of the design of experiments results showing the influence of temperature, reaction time and ferrate concentration on the vanillic acid yield. Left:  $c(\text{ferrate}) = 0.1 \text{ g L}^{-1}$ , right:  $c(\text{ferrate}) = 1.5 \text{ g L}^{-1}$ .

170 °C was chosen. The ferrate was freshly produced before the lignosulfonate degradation under the previously described conditions. Concentrations of ferrate were prepared in the range of 0.1 and 1.5 g L<sup>-1</sup> for DoE experiments. The exact ferrate concentration was determined after electrolysis via UV/Vis measurements after diluting the solution with NaOH as needed.

After the reactions and subsequent workup, vanillic acid (**1**) was detected via LC-MS as the dominant low molecular weight product (Figure 7) in all 34 experiments conducted.

The DoE results (Figure 4) indicated that the reaction temperature and the degradation time play a crucial role in the degradation process (see also Tables S5–S7, Supporting Information). The temperature profile showed an almost linear behavior, resulting in a higher vanillic acid yield with increasing temperatures (see also Figure S2c,d, Supporting Information). Also, prolonged degradation times positively influenced the yield, but an apparent asymptotic behavior toward higher values can be observed (see also Figure S2a,b, Supporting Information). Higher ferrate concentration (Figure 4 right,  $c(\text{ferrate}) = 1.5 \text{ g L}^{-1}$ ) yielded more vanillic acid (see also Figure S2e,f, Supporting Information). The DoE optimization suggested 170 °C, 16 h, and 1.5 g L<sup>-1</sup> ferrate as reaction conditions for achieving the highest vanillic acid yield. Using the green oxidizer ferrate, vanillic acid was obtained in a yield of 7.2 wt% related to the initial lignosulfonate mass, an improvement of almost 1 wt% (12.5% overall increase) in comparison to pure thermal alkaline treatment without ferrate. The conversion shows an exclusive selectivity for vanillic acid, which is directly obtainable from lignin during degradation in 40 wt% NaOH. No other significant low molecular weight products, for example, vanillin, were observed.

One more advantage is that ferrate reacts to iron oxide, which then precipitates and can be easily removed. Therefore, only vanillic acid is obtained as the product in the organic layer upon workup. With these reactions, it was possible to show the positive oxidative effect of ferrate on lignosulfonate degradation. The comparisons between reactions in 40 wt% NaOH show (Table 1) that vanillic acid is not formed by oxidation of vanillin with ferrate but due to the high base concentrations. Ferrate is most likely oxidizing the lignosulfonate or subsequent oligomers, which appears to be beneficial for degradation efficiency. This hypothesis is supported by density functional theory (DFT) calculations performed by Beckham et al. The authors predicted that oxidation of primary

and secondary alcohol groups on alkyl chains of lignin would lower the bond dissociation enthalpy, thereby improving conversion rates.<sup>[74]</sup> Therefore, the thermal treatment supports the bond cleavage to obtain vanillic acid. Other lignin types were also tested to present the practical nature of this new method using ferrate. The optimal conditions obtained from the DoE for lignosulfonate were also applied to Kraft lignin and organosolv lignin. Ferrate showed an improvement in Kraft lignin degradation (0.7 wt%; 175% overall) but had no impact on organosolv lignin (Table 1). This may be because the potential vanillin content is much lower than in Kraft lignin or lignosulfonate.

### 3. Conclusion

We successfully implemented the ferrate oxidation on different types of technically relevant lignins at elevated temperatures. This way, we found a highly selective degradation pathway to the lignin-originating new product—vanillic acid. The ferrate generation was optimized regarding NaOH concentration and current density, which revealed passivation of the GCI electrodes due to persistent carbon deposits, especially at  $j = 100 \text{ mA cm}^{-2}$ . These findings indicate that the material is not ideally suited for long-term ferrate generation at constant current efficiencies. Ferrate assisted the lignin degradation generating vanillic acid in almost exclusive selectivity starting from

**Table 1.** Degradation of various types of lignins without and with ferrate. The optimized conditions were used: 40 wt% NaOH, 170 °C, 16 h reaction time, and 1.5 g L<sup>-1</sup> ferrate.

Type of lignin	Vanillic acid ( <b>1</b> ) <sup>a)</sup>
Lignosulfonate (without ferrate)	6.4 wt% ± 0.1 wt%
Lignosulfonate	7.2 wt% ± 0.1 wt%
Fraunhofer Kraft lignin (without ferrate)	4 wt% ± 0.1 wt%
Fraunhofer Kraft lignin	4.7 wt% ± 0.1 wt%
Fraunhofer organosolv lignin (without ferrate)	2 wt% ± 0.1 wt%
Fraunhofer organosolv lignin	2 wt% ± 0.1 wt%

<sup>a)</sup>The yield of **1** is related to the amount of starting material and was determined by HPLC with 1,3-dimethoxybenzene as the internal standard.

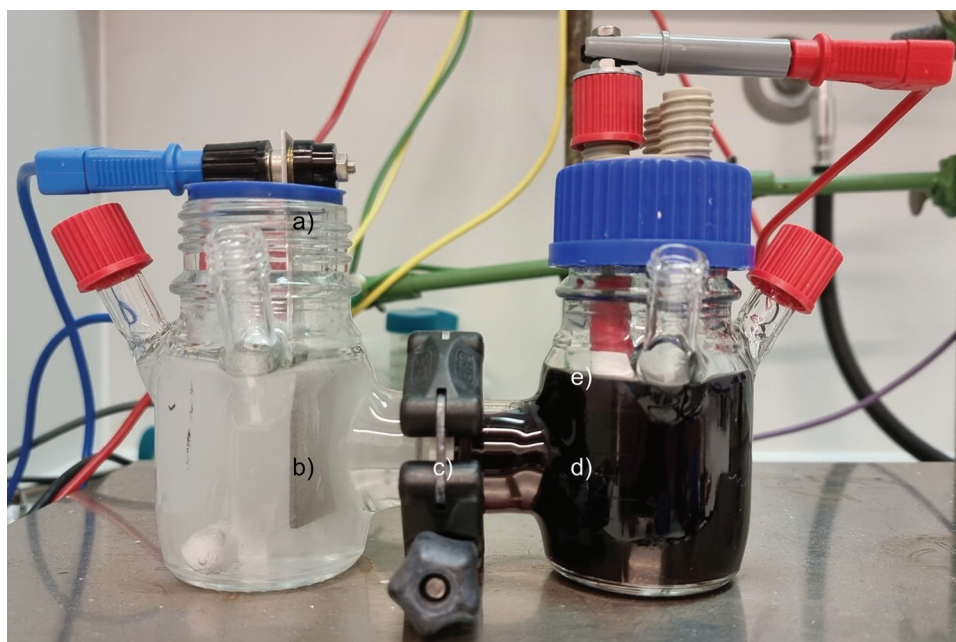


**Figure 5.** H-cell batch reactor: a) stainless steel cathode, b) cathodic chamber with catholyte, c) flange with cation exchange membrane, d) anodic chamber with anolyte, and e) GCI anode.

lignosulfonate. Ferrate increased the yield by 0.8 to 7.2 wt%. While the reaction time already showed asymptotic behavior at 16 h, the temperature and ferrate concentration show an almost linear influence on vanillic acid yield.

#### 4. Experimental Section

**Electrochemical Reactor Setup:** Electrolysis was performed in an H-cell batch reactor made from glass in which the anodic and cathodic chambers were divided by a Nafion N324 cation exchange membrane (Chemours, Fayetteville, U.S.A.). Both chambers had net volumes of 100 mL each.

The anodic chamber was equipped with a GCI rod electrode (0.6025: C = 3.20–3.50 wt%, Si = 2.5–2.7 wt%, Mn = 0.50–0.80 wt%, P = 0.10–0.20 wt%, S = 0.10 wt%, Cu = 0.10–0.60 wt%) with 10 cm<sup>2</sup> surface area ( $d = 10$  mm,  $h = 30$  mm). A stainless-steel plate (1.4301) in the dimensions 30 mm × 25 mm × 2 mm, resulting in a 15 cm<sup>2</sup> surface area, was used as the counter electrode. The distance between the electrodes was 8 cm. Electrolysis experiments were carried out under galvanostatic conditions using Rohde & Schwarz HMP4040 and NGP804 power supplies (Rohde & Schwarz GmbH & Co. KG, Munich, Germany) (Figure 5).

**Electrochemical Synthesis and Quantification of Dissolved Ferrate:** GCI acted as a sacrificial anode to produce ferrate and got dissolved in the process, leading to changes in surface properties. All GCI-electrodes were cut from a single GCI block using electrical discharge machining

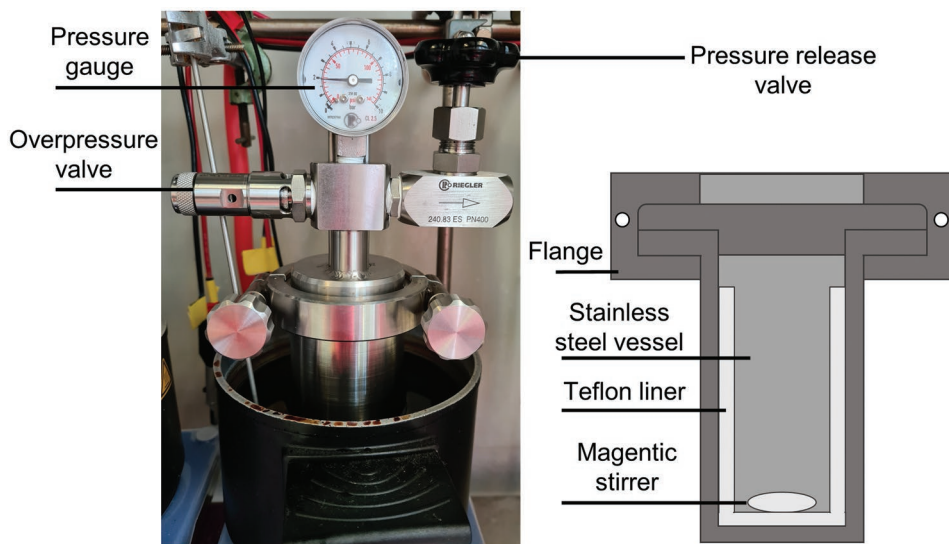


**Figure 6.** Left: Autoclave in operation, right: cross-section of the autoclave.

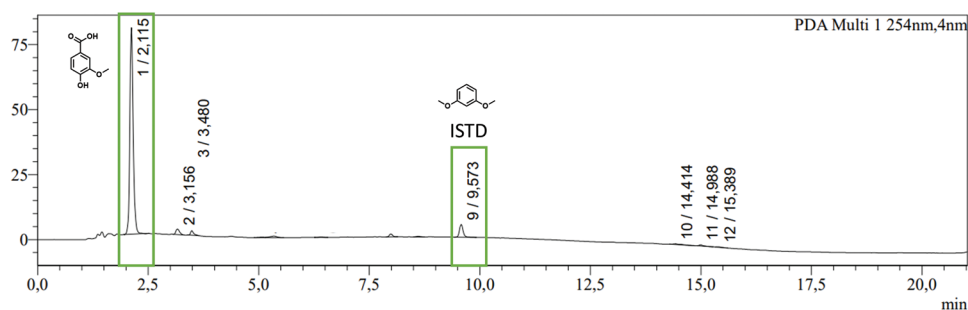


**Figure 7.** HPLC analysis of crude mixture after the ferrate oxidation of liginosulfonate. ISTD: 1,3-dimethoxybenzene.

(EDM) and polished on a lathe afterward to increase reproducibility. Before use, samples were etched with a mixture of 3.5 g L<sup>-1</sup> urotropine in 18.5% HCl for 10 min to remove ferric oxides on the electrode surface. After this procedure, they were treated in an ultrasonic bath in Millipore water for a further 10 min. For better comparison, every electrode was used only once. All experiments were conducted in triplicates. The electrolyte temperatures were not measured or adjusted; however, the experiments were conducted in a temperature-controlled room, guaranteeing the same room temperature each day.

Electro-generation of ferrate using GCI (0.6025) was optimized by testing different concentrations of NaOH (10, 20, 30, 40, and 50 wt%) at an anodic current density of  $j_{an.} = 50 \text{ mA cm}^{-2}$  for 2 h. Based on these results, 40 wt% NaOH was identified as the best electrolyte out of the five tested concentrations and used for further studies. In addition, the influence of anodic current densities on the electrochemical ferrate synthesis was tested in 40 wt% NaOH for 5 h at  $j_{an.} = 25, 50, 75,$  and  $100 \text{ mA cm}^{-2}$ , respectively.

Dissolved ferrate was quantified using direct UV/Vis spectroscopy by measuring the peak at 510 nm. Samples collected during electrolysis were transferred to a microwell plate (UltraCruz UV Transparent Microplates 96 well, flat bottom, Santa Cruz Biotechnology, Inc., Dallas, U.S.A.) and diluted with the corresponding concentration of NaOH if necessary. The optical density of the 100  $\mu\text{L}$  sample was determined in the microwell plate using a Tecan Spark multimode microplate reader (Tecan Group Ltd., Männedorf, Switzerland).

The optical density measurements were used to calculate the ferrate concentration based on previously produced linear calibration graphs (Figures S24–S30, Supporting Information). These were obtained by preparing a dilution series of self-made ferrate produced using the conditions mentioned above and measuring the optical density of the series. The initial concentration of ferrate in the solution was determined with ICP-OES after centrifugation, assuming that ferrate is the only source of iron present. Considering the very poor solubility of iron and iron oxides in NaOH, this presented the most convenient solution to precisely determine the iron content.

**Current Efficiency Calculation Methods:** The current efficiency of electrochemically produced ferrate was calculated as the ratio between ferrate measured during the experiments and the theoretically possible amount of ferrate.

$$\text{current efficiency} = \frac{m(\text{ferrate})_{\text{experimental}}}{m(\text{ferrate})_{\text{theoretical}}} \quad (1)$$

The possible theoretical amount of electro-generated ferrate was calculated according to Faraday's law

$$m(\text{ferrate}) = \frac{MIt}{zF} \quad (2)$$

where  $M$  is the molecular weight of ferrate (119.84 g mol<sup>-1</sup>),  $I$  is the applied current (A),  $t$  is the time (s),  $z$  is the number of electrons involved in the reaction (6 e<sup>-</sup>), and  $F$  is the Faraday constant (96485 C mol<sup>-1</sup>).

**Experimental Setup of Lignin Degradation:** High-temperature experiments were conducted in a simple undivided 0.05 L stainless steel cell with a Teflon liner (Figure 6). The cell was sealable with a flange and equipped with a manometer, a pressure release, and an over-pressure valve (8 bar). The reaction mixture was stirred by a magnetic stirrer. Heating was facilitated by a common oil bath using a standard electric heating plate. A glass pressure tube was also suitable for shorter reaction times (up to 2 h). However, after 2 h, the caustic soda might attack the glass.

**Thermal Degradation of Lignosulfonate with Ferrate:** 250 mg liginosulfonate was dissolved in an aqueous ferrate solution (0.1 to 1.5 g L<sup>-1</sup> in 40 wt% NaOH, 50 mL) under vigorous stirring. Ferrate was always measured before via UV/Vis to determine the concentration. UV/Vis was performed on a Lambda 16, double-beam spectrophotometer (Perkin-Elmer, Waltham, U.S.A.). The software used was UV-Winlab by Perkin-Elmer. A 0.5 cm quartz cuvette was used to make the measurements. The samples collected (0.1 mL) from the ferrate reaction were diluted with 1.4 mL caustic soda and measured without additional procedures.

After the concentration determination, the ferrate solution was transferred into the autoclave; the cell was sealed and stirred at different temperatures (140 to 170 °C) for 2 to 16 h. The reactor was not pressurized externally. After the reaction was stopped, the reaction mixture was allowed to cool (room temperature), and the pH value of the reaction mixture was adjusted to pH 1 by adding HCl. The aqueous layer was extracted with ethyl acetate (3 × 150 mL). The combined organic fractions were dried over anhydrous magnesium sulfate, followed by solvent removal under reduced pressure. The organic residue was dissolved in 8 mL ethyl acetate, 20  $\mu\text{L}$  of the internal standard dimethylbenzene was added, and the sample was analyzed via HPLC/HPLC-MS (Shimadzu, further information provided in Supporting Information) (Figure 7).

## Supporting Information

Supporting Information is available from the Wiley Online Library or from the author.

## Acknowledgements

J. K. and R. K. contributed equally to this work. The authors gratefully acknowledge the support of Borregaard ASA and Fraunhofer Germany. Support from the Forschungsinitiative des Landes Rheinland-Pfalz in frame of SusInnoScience is highly appreciated. Furthermore, the authors gratefully acknowledge the financial support from the German Federal Ministry of Economic Affairs and climate action (number IGF 21766 N/1) and the Norwegian research council through the project Lignin to BioAromatics (321427). Finally, the authors thank Ediz Duman for reproducing measurements during his master's thesis.

Open access funding enabled and organized by Projekt DEAL.



## Conflict of Interest

The authors declare no conflict of interest.

## Data Availability Statement

The data that support the findings of this study are available in the supplementary material of this article.

## Keywords

electrochemistry, ferrate, lignin, liginosulfonate, vanillic acid

Received: October 8, 2022

Revised: November 16, 2022

Published online: December 25, 2022

- [1] a) C. Chio, M. Sain, W. Qin, *Renewable Sustainable Energy Rev.* **2019**, *107*, 232; b) H. Wang, Y. Pu, A. Ragauskas, B. Yang, *Bioresour. Technol.* **2019**, *271*, 449; c) K. Chen, M. Cao, C. Ding, X. Zheng, *RSC Adv.* **2018**, *8*, 26782; d) S. Dutta, K. C.-W. Wu, B. Saha, *Catal. Sci. Technol.* **2014**, *4*, 3785; e) W. Boerjan, J. Ralph, M. Baucher, *Annu. Rev. Plant Biol.* **2003**, *54*, 519; f) A. Das, A. Rahimi, A. Ulbrich, M. Alherech, A. H. Motagamwala, A. Bhalla, L. da Costa Sousa, V. Balan, J. A. Dumesic, E. L. Hegg, B. E. Dale, J. Ralph, J. J. Coon, S. S. Stahl, *ACS Sustainable Chem. Eng.* **2018**, *6*, 3367.
- [2] D. S. Bajwa, G. Pourhashem, A. H. Ullah, S. G. Bajwa, *Ind. Crops Prod.* **2019**, *139*, 111526.
- [3] J. Klein, K. Alt, S. R. Waldvogel, *Adv. Sustainable Syst.* **2022**, *6*, 2270010.
- [4] A. J. Ragauskas, G. T. Beckham, M. J. Biddy, R. Chandra, F. Chen, M. F. Davis, B. H. Davison, R. A. Dixon, P. Gilna, M. Keller, P. Langan, A. K. Naskar, J. N. Saddler, T. J. Tschaplinski, G. A. Tuskan, C. E. Wyman, *Science* **2014**, *344*, 1246843.
- [5] F. G. Calvo-Flores, J. A. Dobado, *ChemSusChem* **2010**, *3*, 1227.
- [6] I. Sumerskii, P. Korntner, G. Zinovyev, T. Rosenau, A. Potthast, *RSC Adv.* **2015**, *5*, 92732.
- [7] C. Brandt, *Chem. Unserer Zeit* **2002**, *36*, 214.
- [8] R. Rinaldi, R. Jastrzebski, M. T. Clough, J. Ralph, M. Kennema, P. C. A. Bruijninx, B. M. Weckhuysen, *Angew. Chem., Int. Ed.* **2016**, *55*, 8164; *Angew. Chem.* **2016**, *128*, 8296.
- [9] T. Aro, P. Fatehi, *ChemSusChem* **2017**, *10*, 1861.
- [10] R. Vanholme, B. Demedts, K. Morreel, J. Ralph, W. Boerjan, *Plant Physiol.* **2010**, *153*, 895.
- [11] B. E. Dale, *J. Chem. Technol. Biotechnol.* **2003**, *78*, 1093.
- [12] C. O. Tuck, E. Pérez, I. T. Horváth, R. A. Sheldon, M. Poliakoff, *Science* **2012**, *337*, 695.
- [13] Z. Sun, B. Fridrich, A. de Santi, S. Elangovan, K. Barta, *Chem. Rev.* **2018**, *118*, 614.
- [14] C. Crestini, H. Lange, M. Sette, D. S. Argyropoulos, *Green Chem.* **2017**, *19*, 4104.
- [15] a) M. D. Kärkäs, B. S. Matsuura, T. M. Monos, G. Magallanes, C. R. J. Stephenson, *Org. Biomol. Chem.* **2016**, *14*, 1853; b) M. M. Abu-Omar, K. Barta, G. T. Beckham, J. S. Luterbacher, J. Ralph, R. Rinaldi, Y. Román-Leshkov, J. S. M. Samec, B. F. Sels, F. Wang, *Energy Environ. Sci.* **2021**, *14*, 262; c) M. Garede, C. H. Lam, L. Petitjean, S. Huang, B. Song, F. Lin, J. E. Jackson, C. M. Saffron, P. T. Anastas, *Green Chem.* **2021**, *23*, 2868; d) S. Constant, H. L. J. Wienk, A. E. Frissen, P. d. Peinder, R. Boelens, D. S. van Es, R. J. H. Grisel, B. M. Weckhuysen, W. J. J. Huijgen, R. J. A. Gosselink, P. C. A. Bruijninx, *Green Chem.* **2016**, *18*, 2651.
- [16] Z. Chen, C. Wan, *Renewable Sustainable Energy Rev.* **2017**, *73*, 610.
- [17] M. A. Ahmed, J. H. Lee, A. A. Raja, J. W. Choi, *Appl. Sci.* **2020**, *10*, 1599.
- [18] O. Y. Abdelaziz, D. P. Brink, J. Prothmann, K. Ravi, M. Sun, J. García-Hidalgo, M. Sandahl, C. P. Hultberg, C. Turner, G. Lidén, M. F. Gorwa-Grauslund, *Biotechnol. Adv.* **2016**, *34*, 1318.
- [19] M. Zirbes, D. Schmitt, N. Beiser, D. Pitton, T. Hoffmann, S. R. Waldvogel, *ChemElectroChem* **2019**, *6*, 155.
- [20] L. Das, P. Kolar, R. Sharma-Shivappa, J. J. Classen, J. A. Osborne, *Waste Biomass Valorization* **2017**, *8*, 2673.
- [21] M. Breiner, M. Zirbes, S. R. Waldvogel, *Green Chem.* **2021**, *23*, 6449.
- [22] a) M. B. Hocking, *J. Chem. Educ.* **1997**, *74*, 1055; b) D. Schmitt, C. Regenbrecht, M. Hartmer, F. Stecker, S. R. Waldvogel, *Beilstein J. Org. Chem.* **2015**, *11*, 473; c) D. Schmitt, C. Regenbrecht, M. Schubert, D. Schollmeyer, S. R. Waldvogel, *Holzforchung* **2017**, *71*, 35.
- [23] A. Rahimi, A. Ulbrich, J. J. Coon, S. S. Stahl, *Nature* **2014**, *515*, 249.
- [24] M. Zirbes, S. R. Waldvogel, *Curr. Opin. Green Sustainable Chem.* **2018**, *14*, 19.
- [25] a) B. Biannic, J. J. Bozell, *Org. Lett.* **2013**, *15*, 2730; b) J. C. Wozniak, D. R. Dimmel, E. W. Malcolm, *J. Wood Chem. Technol.* **1989**, *9*, 491.
- [26] A. Agarwal, M. Rana, J.-H. Park, *Fuel Process. Technol.* **2018**, *181*, 115.
- [27] H. Zhu, L. Wang, Y. Chen, G. Li, H. Li, Y. Tang, P. Wan, *RSC Adv.* **2014**, *4*, 29917.
- [28] a) J. Zhang, J. Teo, X. Chen, H. Asakura, T. Tanaka, K. Teramura, N. Yan, *ACS Catal.* **2014**, *4*, 1574; b) Y. Zhai, C. Li, G. Xu, Y. Ma, X. Liu, Y. Zhang, *Green Chem.* **2017**, *19*, 1895; c) S. Li, W. Li, Q. Zhang, R. Shu, H. Wang, H. Xin, L. Ma, *RSC Adv.* **2018**, *8*, 1361; d) S. Qiu, M. Li, Y. Huang, Y. Fang, *Ind. Eng. Chem. Res.* **2016**, *57*, 2023; e) X. Zhang, W. Tang, Q. Zhang, Y. Li, L. Chen, Y. Xu, C. Wang, L. Ma, *Fuel* **2018**, *215*, 825; f) M. Grilc, B. Likozar, J. Levec, *Appl. Catal., B* **2014**, *150-151*, 275.
- [29] a) C. Hardacre, V. Parvulescu (Hrsg) in *Catalysis Series*, Royal Society of Chemistry, London **2014**, p. 289; b) K. Stärk, N. Taccardi, A. Bösmann, P. Wasserscheid, *ChemSusChem* **2010**, *3*, 719; c) Y. Yang, H. Fan, Q. Meng, Z. Zhang, G. Yang, B. Han, *Chem. Commun. (Cambridge, U. K.)* **2017**, *53*, 8850; d) J. Zakzeski, P. C. A. Bruijninx, B. M. Weckhuysen, *Green Chem.* **2011**, *13*, 671.
- [30] M. Zirbes, L. L. Quadri, M. Breiner, A. Stenglein, A. Bomm, W. Schade, S. R. Waldvogel, *ACS Sustainable Chem. Eng.* **2020**, *8*, 7300.
- [31] D. Di Marino, T. Jestel, C. Marks, J. Viell, M. Blindert, S. M. A. Kriescher, A. C. Spiess, M. Wessling, *ChemElectroChem* **2019**, *6*, 1434.
- [32] a) J. Seidler, J. Strugatchi, T. Gärtner, S. R. Waldvogel, *MRS Energy Sustain.* **2020**, *7*, E42; b) S. B. Beil, D. Pollok, S. R. Waldvogel, *Angew. Chem., Int. Ed.* **2021**, *60*, 14750; *Angew. Chem.* **2021**, *133*, 14874; c) D. Pollok, S. R. Waldvogel, *Chem. Sci.* **2020**, *11*, 12386; d) M. Yan, Y. Kawamata, P. S. Baran, *Chem. Rev.* **2017**, *117*, 13230; e) S. Möhle, M. Zirbes, E. Rodrigo, T. Gieshoff, A. Wiebe, S. R. Waldvogel, *Angew. Chem., Int. Ed.* **2018**, *57*, 6018; *Angew. Chem.* **2018**, *130*, 6124; f) K. D. Moeller, *Chem. Rev.* **2018**, *118*, 4817; g) H. J. Schäfer, *C. R. Chim.* **2011**, *14*, 745; h) B. A. Frontana-Uribe, R. D. Little, J. G. Ibanez, A. Palma, R. Vasquez-Medrano, *Green Chem.* **2010**, *12*, 2099; i) S. R. Waldvogel, B. Janza, *Angew. Chem., Int. Ed.* **2014**, *53*, 7122; *Angew. Chem.* **2014**, *126*, 7248; j) P. Anastas, N. Eghbali, *Chem. Soc. Rev.* **2010**, *39*, 301; k) J. Homann, M. Zirbes, M. Arndt-Engelbart, D. Scholz, S. R. Waldvogel, T. Hoffmann, *ChemElectroChem* **2022**, *9*, 202101312.
- [33] a) R. H. J. Creighton, R. D. Gibbs, H. Hibbert, *J. Am. Chem. Soc.* **1944**, *66*, 32; b) J. C. Villar, A. Caperos, F. García-Ochoa, *J. Wood Chem. Technol.* **1997**, *17*, 259.
- [34] T. P. Schultz, M. C. Templeton, *Holzforchung* **1986**, *40*, 93.
- [35] a) E. I. Evstigneyev, O. S. Yuzikhin, A. A. Gurinov, A. Y. Ivanov, T. O. Artamonova, M. A. Khodorkovskiy, E. A. Bessonova,

- A. V. Vasilyev, *J. Wood Chem. Technol.* **2016**, 36, 259; b) J. A. Jennings, S. Parkin, E. Munson, S. P. Delaney, J. L. Calahan, M. Isaacs, K. Hong, M. Crocker, *RSC Adv.* **2017**, 7, 25987; c) Q. Xiang, Y. Y. Lee, *Appl. Biochem. Biotechnol.* **2000**, 84, 153.
- [36] L. Ninane, N. Kanari, C. Criado, C. Jeannot, O. Evrard, N. Neveux, in *ACS Symposium Series (Hrsg.: V. K. Sharma)*, American Chemical Society, Washington, DC **2008**, pp. 102–111.
- [37] G. W. Thompson, L. T. Ockerman, J. M. Schreyer, *J. Am. Chem. Soc.* **1951**, 73, 1379.
- [38] V. K. Sharma, R. Zboril, R. S. Varma, *Acc. Chem. Res.* **2015**, 48, 182.
- [39] S. Wang, Z. Yang, D. Liu, S. Wang, *Electrochim. Acta* **2010**, 55, 1985.
- [40] M. Diaz, K. Doederer, J. Keller, M. Cataldo, B.-C. Donose, Y. Ali, P. Ledezma, *J. Electroanal. Chem.* **2021**, 880, 114897.
- [41] a) M. Diaz, M. Cataldo, P. Ledezma, J. Keller, K. Doederer, *J. Electroanal. Chem.* **2019**, 854, 113501; b) V. K. Sharma, G. W. Luther, F. J. Millero, *Chemosphere* **2011**, 82, 1083; c) C. Li, X. Z. Li, N. Graham, N. Y. Gao, *Water Res.* **2008**, 42, 109; d) J. Q. Jiang, *J. Hazard. Mater.* **2007**, 146, 617; e) C. He, X.-Z. Li, V. K. Sharma, S.-Y. Li, *Environ. Sci. Technol.* **2009**, 43, 5890; f) L. Hu, H. M. Martin, O. Arce-Bulted, M. N. Sugihara, K. A. Keating, T. I. Strathmann, *Environ. Sci. Technol.* **2009**, 43, 509; g) Y. Lee, U. von Gunten, *Water Res.* **2010**, 44, 555; h) V. K. Sharma, *J. Environ. Sci. Health, Part A: Toxic/Hazard. Subst. Environ. Eng.* **2010**, 45, 645; i) A. A. Dar, B. Pan, J. Qin, Q. Zhu, E. Lichtfouse, M. Usman, C. Wang, *Environ. Pollut.* **2021**, 290, 117957; j) H. Wang, L. E. Block, R. D. Rogers, in *Catalysis Series (Hrsg.: C. Hardacre, V. Parvulescu)*, Royal Society of Chemistry, London **2014**, p. 1.
- [42] K. M. Wang, J. Shu, S. J. Wang, T. Y. Hong, X. P. Xu, H. Y. Wang, *J. Hazard. Mater.* **2020**, 384, 121458.
- [43] R. Pi, H. Liu, X. Sun, R. Zhang, J. Zhang, V. K. Sharma, *Sep. Purif. Technol.* **2021**, 263, 671.
- [44] a) P. Nguema, M. jun, *Int. J. Microbiol. Res.* **2016**, 7, 53; b) Y. Lee, S. G. Zimmermann, A. T. Kieu, U. von Gunten, *Environ. Sci. Technol.* **2009**, 43, 3831; c) A. Talaiekhazani, M. R. Talaei, S. Rezaia, *J. Environ. Chem. Eng.* **2017**, 5, 1828.
- [45] N. Graham, C.-C. Jiang, X.-Z. Li, J.-Q. Jiang, J. Ma, *Chemosphere* **2004**, 56, 949.
- [46] P. C. W. Cheung, D. R. Williams, J. Barrett, J. Barker, D. W. Kirk, *Molecules* **2021**, 26, 5266.
- [47] M. Alsheyab, J.-Q. Jiang, C. Stanford, *J. Environ. Manage.* **2009**, 90, 1350.
- [48] V. Lescuras-Darrou, F. Lopicque, G. Valentin, *J. Appl. Electrochem.* **2002**, 32, 57.
- [49] K. Bouzek, I. Roušar, M. A. Taylor, *J. Appl. Electrochem.* **1996**, 26, 925.
- [50] K. Bouzek, I. Roušar, *J. Appl. Electrochem.* **1993**, 23, 1317.
- [51] K. Bouzek, I. Roušar, *J. Appl. Electrochem.* **1996**, 26, 919.
- [52] K. Bouzek, I. Rousar, *J. Appl. Electrochem.* **1997**, 27, 679.
- [53] X. Sun, Q. Zhang, H. Liang, L. Ying, M. Xiangxu, V. K. Sharma, *J. Hazard. Mater.* **2016**, 319, 130.
- [54] K. Bouzek, I. Rousar, M. A. Taylor, *J. Appl. Electrochem.* **1996**, 26, 925.
- [55] M. Gitzinger, C. Kemmer, D. A. Fluri, M. D. El-Baba, W. Weber, M. Fussenegger, *Nucleic Acids Res.* **2012**, 40, e37.
- [56] N. S. Chatterjee, S. K. Panda, M. Navitha, K. K. Asha, R. Anandan, S. Mathew, *J. Food Sci. Technol.* **2015**, 52, 7153.
- [57] a) P. S. M. Prince, S. Rajakumar, K. Dhanasekar, *Eur. J. Pharmacol.* **2011**, 668, 233; b) S.-J. Kim, M.-C. Kim, J.-Y. Um, S.-H. Hong, *Molecules* **2010**, 15, 7208.
- [58] N. J. Walton, M. J. Mayer, A. Narbad, *Phytochemistry* **2003**, 63, 505.
- [59] A. L. Pometto, D. L. Crawford, *Appl. Environ. Microbiol.* **1983**, 45, 1582.
- [60] J. Wenger, V. Haas, T. Stern, *Curr. For. Rep.* **2020**, 6, 294.
- [61] I. A. Pearl, *J. Am. Chem. Soc.* **1946**, 68, 429.
- [62] I. A. Pearl, *J. Am. Chem. Soc.* **1946**, 68, 1100.
- [63] T. Sabalitschka, *Arch. Pharm. Pharm. Med. Chem.* **1931**, 269, 545.
- [64] a) M. Maeda, T. Hosoya, K. Yoshioka, H. Miyafuji, H. Ohno, T. Yamada, *J. Wood Sci.* **2018**, 64, 810; b) T. Rinesch, J. Mottweiler, M. Puche, P. Concepción, A. Corma, C. Bolm, *ACS Sustainable Chem. Eng.* **2017**, 5, 9818; c) R. Delisi, R. Ciriminna, F. Parrino, L. Palmisano, Y.-J. Xu, M. Pagliaro, *ChemistrySelect* **2016**, 1, 626.
- [65] a) P. Barghini, F. Montebove, M. Ruzzi, A. Schiesser, *Appl. Microbiol. Biotechnol.* **1998**, 49, 309; b) A. Muheim, K. Lerch, *Appl. Microbiol. Biotechnol.* **1999**, 51, 456.
- [66] M. Klein, S. R. Waldvogel, *Angew. Chem., Int. Ed.* **2022**, 61, e202204140; *Angew. Chem.* **2022**, 134, e202204140.
- [67] Z. Mácová, K. Bouzek, *J. Appl. Electrochem.* **2012**, 42, 615.
- [68] Lehn, F. Chris, Chemical solution dispenser apparatus and method of use thereof (EP0229038 A2) **1987**.
- [69] Z. Mácová, K. Bouzek, J. Híveš, V. K. Sharma, R. J. Terryn, J. C. Baum, *Electrochim. Acta* **2009**, 54, 2673.
- [70] G. Wulfsberg, *Inorganic Chemistry*, University Science Books, Sausalito, CA **2000**.
- [71] L. Longe, G. Garnier, K. Saito, *Molecules* **2019**, 24, 3717.
- [72] K. Freudenberg, W. Lautsch, K. Engler, *Ber. Dtsch. Chem. Ges.* **1940**, 73, 167.
- [73] M. Dörr, M. M. Hielscher, J. Proppe, S. R. Waldvogel, *ChemElectroChem* **2021**, 8, 2621.
- [74] S. Kim, S. C. Chmely, M. R. Nimlos, Y. J. Bomble, T. D. Foust, R. S. Paton, G. T. Beckham, *J. Phys. Chem. Lett.* **2011**, 2, 2846.